PAPER

Experimental and theoretical study on the dissociative photoionization of methyl methacrylate

IOP Publishing Journal of Physics B: Atomic, Molecular and Optical Physics
J. Phys. B: At. Mol. Opt. Phys. **50** (2017) 235101 (11pp) https://doi.org/10.1088/1361-6455/aa92d4

Experimental and theoretical study on the dissociative photoionization of methyl methacrylate

Ruirui Sun[1], Qinghui Meng[1], Ming Wang[1], Weifei Fei[1], Yanmei Zhang[1], Jun Chen[1], Wenzheng Fang[1,2], Xiaobin Shan[1], Fuyi Liu[1] and Liusi Sheng[1]

[1] National Synchrotron Radiation Laboratory, School of Nuclear Science and Technology, University of Science and Technology of China, Hefei, Anhui 230029, People's Republic of China
[2] Section for Earth and Environmental Sciences, Department of Environmental Science and Analytical Chemistry, Bolin Centre for Climate Research, Stockholm University, Svante Arrhenius Väg 8, Stockholm, SE-10691, Sweden

E-mail: jchenah@mail.ustc.edu.cn

Received 12 January 2017, revised 10 October 2017
Accepted for publication 12 October 2017
Published 8 November 2017

Abstract

The photoionization of methyl methacrylate and dissociation of its cation have been investigated by tunable vacuum ultraviolet synchrotron radiation coupled with time-of-flight mass spectrometer in the photon energy region of 9.0–15.5 eV. The ionization energy of methyl methacrylate and the appearance energies (AEs) for major fragments, $C_5H_7O_2^+$, $C_5H_6O^+$, $C_4H_5O_2^+$, $C_4H_5O^+$, $C_3H_4O^+$, $C_3H_3O^+$ ($C_4H_7^+$), $C_3H_5^+$, $C_3H_4^+$, $C_2H_3O_2^+$, and CH_3^+ are determined to be 9.76, 10.30, 10.66, 10.51, 11.17, 10.51, 10.74, 12.88, 12.73, 12.52, and 12.82 eV, respectively, by measurement of the photoionization efficiency curves. Possible formation pathways of the major fragments are proposed based on comparison of experimental AEs and energies predicted by *ab initio* G3B3 calculations. Transition states and intermediates involved in the dissociation channels are also located. The majority of the proposed channels occur through isomerization prior to dissociation. Hydrogen shift and ring closing/opening are found to be the dominant processes during photofragmentaion of methyl methacrylate.

Supplementary material for this article is available online

Keywords: methyl methacrylate, synchrotron radiation, mass spectrometry, dissociative photoionization, *ab initio* calculations

(Some figures may appear in colour only in the online journal)

1. Introduction

Methyl methacrylate (CH_2=C(CH_3)$COOCH_3$, MMA) is known as the monomer of poly(methyl methacrylate) (PMMA), a colorless polymer which has been widely used in the industry. In the production and use of MMA, it can be easily released into environment due to high vapor pressure [1] and over 2.04×10^9 kg MMA has been produced during industrial processes currently [2]. Up to now, considerable efforts have been made on the degradation and combustion of PMMA and they all reach a similar conclusion that MMA is the most important intermediate during those processes [3–5], which will contribute to the concentration of MMA in the atmosphere. MMA can undergo further transformation or degradation with OH radicals during daytime and nitrate radicals and ozone molecules during nighttime [6, 7], leading to the formation of secondary aerosols in the troposphere. In general, MMA has become a pollutant of environmental concern due to its toxicity, high volatility and large emission [7]. Many previous studies have been mainly focused on the transformation mechanism and reaction rate constants of MMA with OH, NO_3 radicals or O_3 and Cl atoms in the atmosphere [8–11].

Despite these numerous studies performed, some physical properties of MMA, such as its ionization energy (IE) and the appearance energies of the fragment ions, are still not definitely determined. To the best of our knowledge, there have been only three photoionization studies [12–14] about MMA wherein only the IE as well as photoionization cross sections of MMA and its fragments have been determined. Therefore, the detailed dissociative photoionization of MMA is still less understood both experimentally and theoretically. In this paper, a study of dissociative photoionization of MMA is performed using tunable synchrotron vacuum ultraviolet (VUV) coupled with photoionization mass spectrometry (PIMS) in the energy region of 9.0–15.5 eV. The IE of MMA molecule and appearance energies (AEs) of major fragment ions are obtained by measurements of the PIE spectra. Dissociative photoionization channels are proposed and discussed in detail on the basis of experimental measurements and theoretical calculations.

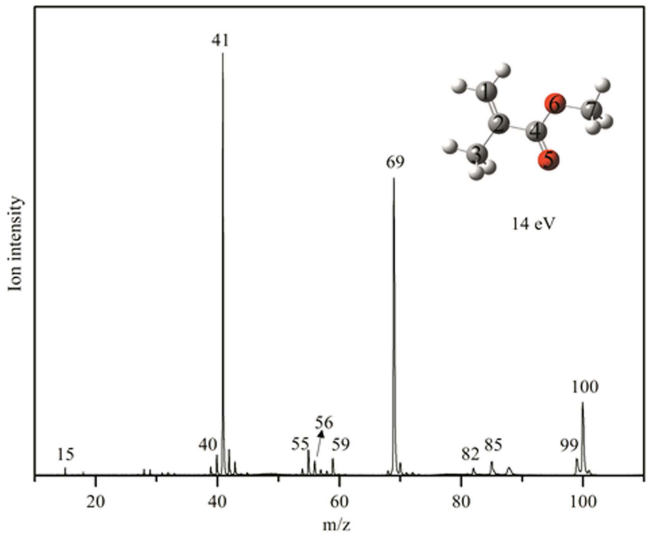

Figure 1. Photoionization mass spectrum of MMA at photon energy of 14 eV. Also shown are the molecular structure of MMA and numeration of carbon and oxygen atoms therein.

2. Experimental methods

2.1. Mass spectrometry details

All experiments were carried out at the Atomic and Molecular Physics Beamline (U14-A), National Synchrotron Radiation Laboratory, Hefei, China. Detailed information about the experimental apparatus has been described elsewhere previously [15–17]. Briefly, PIMS measurements have been performed on a reflectron time-of-flight mass spectrometer instrument under supersonic jet expansion condition by using VUV synchrotron radiation (SR) coming from the undulator of the 800 MeV electron storage ring as a soft ionization source. The SR beam is diffracted by three interchangeable spherical gratings providing photon energies from 7.5 to 124 eV. Before entering the end-station, the beam is refocused by a toroidal focusing mirror after passing through the adjustable exit silt. In this study, only the 370 grooves mm^{-1} grating covering the energy region 7.5–22.5 eV is used. A rare-gas harmonic filter filled with argon is inserted into the beamline in order to eliminate the contamination of higher order harmonics. The average photon flux is measured to be about 10^{12} photons s^{-1}.

Liquid MMA sample is obtained commercially with the purity above 99% and used directly without further purification. The MMA sample (vapor pressure = 5.33 kPa at 298 K) sealed in a stainless steel can is carried by Ar (purity 99.99%) under operating pressure of 0.1 MPa and expanded into the ionization chamber through a nozzle with a diameter of 70 μm and two skimmers with diameter of 1 mm to form a continuous supersonic molecular beam. The monochromatic VUV radiation intersects perpendicularly with the molecular beam to make the MMA molecule photoionized in the ionization region. Then the generated ions are drawn out of the photoionization region by a pulse extraction field triggered with a pulse generator (DG 535 SRS) and detected by a microchannel plate detector. The signals are counted with a multiscaler P7888 counter after amplification with a VT120C (EG&G, ORTEC) preamplifier and transferred to a computer for further analysis. PIE curves for photoions are measured by scanning the monochromator from 9.0 to 15.5 eV with an energy increment of 30 meV. The photon intensity is monitored with a silicon photodiode (SXUV-100, International Radiation Detectors, Inc.) to normalize the ion signals.

2.2. Computational details

The energies of MMA molecule and pertinent species involved in this work are calculated by quantum chemistry method using Gaussian 09 programs [18]. The geometries of the parent molecule, fragment ions, intermediates and transition states are optimized using density functional method with the B3LYP/6-31G(d) hybrid functional. In order to confirm the nature of the stationary points (local minimum or transition state), normal-mode analyses are carried out at each optimized geometry. The intrinsic reaction coordinate (IRC) calculations are also performed to verify that reactants and products are connected by the desired transition state. Zero-point vibrational energies are obtained by harmonic vibrational frequencies calculations computed at the same level of theory used in the geometry optimization. Accurate energies are obtained at the G3B3 level [19].

3. Results and discussion

3.1. Experimental facts

The photoionization mass spectrum of MMA obtained at 14 eV is shown in figure 1. Compared to the 70 eV electron ionization mass spectrum (EIMS) provided by the National Institute of Standards and Technology (NIST) database [20], it is found that both spectra are of essentially the same fragments although their relative intensities are somewhat different. A medium intensity peak at $m/z = 100$ is assigned to

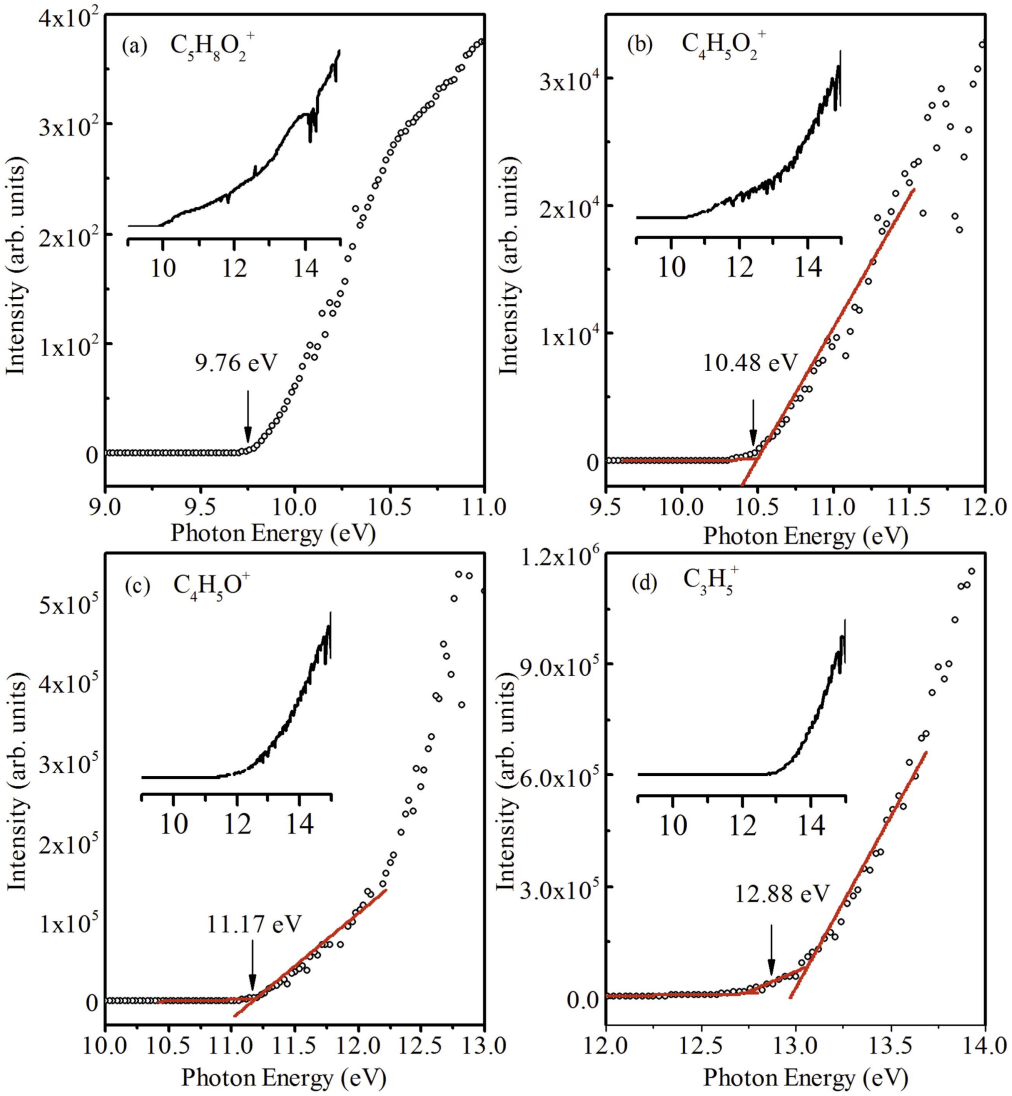

Figure 2. The PIE curves of parent ion $C_5H_8O_2^+$ (a), the main fragments $C_4H_5O_2^+$ (b), $C_4H_5O^+$ (c) and $C_3H_5^+$ (d).

be parent MMA cation $C_5H_8O_2^+$. The higher parent ion intensity in the EIMS might be due to a lower partial cross-section for dissociative ionization in the EI mode caused by inefficient inelastic scattering of the electrons. The $m/z = 41$ ion ($C_3H_5^+$) is the most intense mass peak, followed by the ion with $m/z = 69$ ($C_4H_5O^+$) both in our 14 eV PIMS and in the 70 eV EIMS of the NIST database. Considering the structure of molecular ion of MMA, these two principal fragment ions may arise from C2–C4 and C4–O6 bond scission processes, releasing $COOCH_3$ radical and CH_3O radical, respectively. Additionally, a group of weak peaks at $m/z = 99$, 85, 82, 59, 56, 55, 40, and 15, corresponding to fragments $C_5H_7O_2^+$, $C_4H_5O_2^+$, $C_5H_6O^+$, $C_2H_3O_2^+$, $C_3H_4O^+$, $C_3H_3O^+$ ($C_4H_7^+$), $C_3H_4^+$, and CH_3^+, respectively, can be distinguished clearly as well. All observed fragments are considered to be originated from dissociation of parent ion $C_5H_8O_2^+$ since no signal at mass greater than that of $C_5H_8O_2^+$ ($m/z = 100$) was detected at any excitation energy except for the isotopomer of the molecular ion at $m/z = 101$.

The PIE curves of MMA radical cation and main fragments ions shown in figure 2 are obtained by integrating the area of each mass peak as a function of photon energy, followed by background subtraction and normalization to the photon flux. The normalized signal intensity shown in figure 2 for ion i may be written as $I_i = [I_i\ (m) - I\ (b)]/\Phi_p(E) = \sigma_i(E)ntR_i$. Here, I_i (m) and I (b) are the measured ion intensity and background intensity; $\Phi_p(E)$ is the photon flux; $\sigma_i(E)$ is the photoionization cross-section at the photon energy E; n is the sample gas density; t is spectrum collection time; R_i is mass-dependent response factors that account for sampling and detection efficiency for the target ions. Different approaches have been previously reported to analyze PIE spectra in photoionization studies [21, 22]. For the PIE curves wherein the ion signals increase linearly with IE, a linear fit is employed to the background and to the ion signal. The photon energy at the intersection of these lines is the measured AE value. When the ion signals rise abruptly but with a gradual slow slope in the threshold region, such as $C_3H_5^+$, the AE is determined as the midpoint of the two

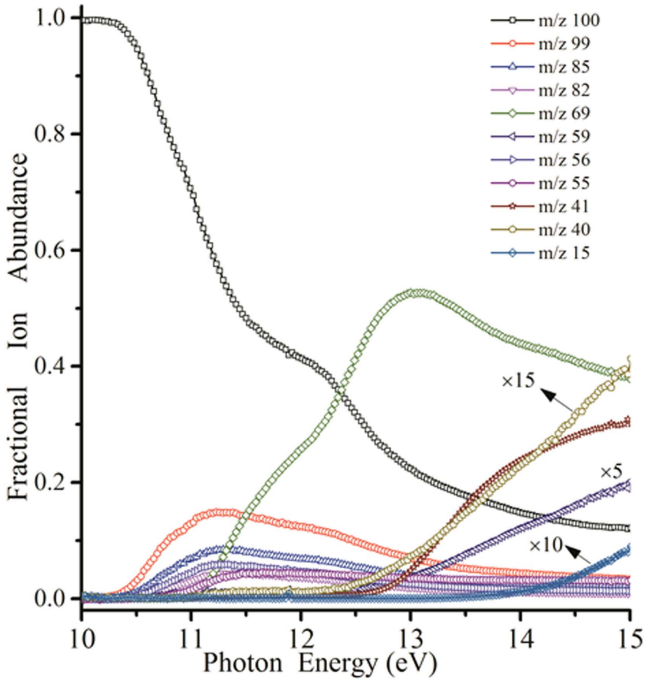

Figure 3. Relative branching ratios of molecular ion of MMA and its major fragment ions as a function of photon energy.

intersects among the rapidly rising line, the slowly rising line, and the background. The AEs of $C_5H_7O_2^+$, $C_5H_6O^+$, $C_4H_5O_2^+$, $C_4H_5O^+$, $C_3H_4O^+$, $C_3H_3O^+$ ($C_4H_7^+$), $C_2H_3O_2^+$, $C_3H_5^+$, $C_3H_4^+$, and CH_3^+ derived from the PIEs are 10.30 ± 0.03, 10.66 ± 0.03, 10.51 ± 0.03, 11.17 ± 0.03, 10.51 ± 0.03, 10.74 ± 0.03, 12.52 ± 0.03, 12.88 ± 0.03, 12.73 ± 0.03 and 12.82 ± 0.03 eV, respectively. For the parent ion, the IE determined from PIE curves (ours and those cited in the discussion) is the adiabatic IE, that is, the energy difference between the ground vibrational and rotational level of the lowest electronic state of the ion and the ground vibrational and rotational level of the lowest electronic state of the molecule. In this study, the IE of $C_5H_8O_2^+$ derived from the PIE curve is 9.76 ± 0.03 eV which is in good agreement with our calculated value 9.77 eV. It should be noted that no correction is made for possible kinetic shifts in determining the AEs. In addition, the thermal energy distribution of parent molecule is not taken into account in data processing, in view of the supersonic jet expansion experimental condition.

The relative branching ratios of the molecular ion of MMA and its major fragment ions as a function of photon energy have been derived from data of PIE curves and are plotted in figure 3. The sum of ion abundances is normalized to 1 at any photon energy. In the energy region of 10–11 eV, the fractional abundance of the molecular ion decreases abruptly while that of fragment ions at m/z 99, 85, 82, 56, and 55 rises, implying that these fragments originate from the molecular ion. Similar analyses for fragment ions at m/z 59, 41, 40, and 15 in the 12–15 eV photon energy region indicate that the first fragment derive from the molecular ion, whereas the latter three species may derive from the molecular ion or fragment at m/z 69 or even both. In addition, the dissociation mechanism of the molecular ion seems to be complicated. Even what appears to be a simple C–H bond rupture reaction, that is, H loss, is very unlikely to occur at an internal energy of only 0.57 eV. The detailed dissociation mechanisms will be discussed later in this study with the aid of theoretical calculations.

3.2. Computational facts

To gain insight into the mechanism of the dissociative photoionization, *ab initio* calculations at the G3B3 level have been carried out as described above. IE is calculated as the total electronic energy difference of the fully optimized cationic and neutral ground state of MMA. AE of fragment ion is defined as $E_{AE} = E_{max} - E_0$, where E_{max} is the highest energy barrier involved in the formation pathway of corresponding fragment ion and E_0 refers to the energy of neutral MMA which is defined to be zero in our study. The dissociation energy (E_d) to produce fragment ion is computed empirically by subtracting the IE of parent molecule from its appearance energy, $E_d = AE - IE$. Experimental and theoretical IE, AEs and E_ds are listed in table 1, along with some possible dissociation channels of MMA. Geometries of species pertinent to this work (neutral molecule, parent ion, fragment cations, transition states, intermediates and radicals) are optimized at G3B3 level and the calculation results are shown in figures S1–S3 (supporting information is available online at stacks.iop.org/JPB/50/235101/mmedia). The bond length is in Å and the angle is in degrees. It is necessary here to give the labeling conventions used throughout the paper in assigning the labels to atoms of MMA. As shown in figure 1, the carbon numbering starts from the methylene group, then proceeds along the $-CCH_3$ moiety. The carbon and oxygen atoms of the carbonyl and $-OCH_3$ group are numbered as C4, O5, O6, and C7, respectively.

3.3. Dissociation mechanisms

In this study, parent ion $C_5H_8O_2^+$ is considered to be formed directly by VUV SR single-photon ionization ($C_5H_8O_2 + h\nu \rightarrow C_5H_8O_2^+ + e$). As the photon energy increases, the parent ion will undergo various dissociation reactions to form fragments. Detailed formation pathways of dominant ionic fragments are established with the aid of calculations at the G3B3 level. The calculated energies of related species are listed in table S1. The proposed fragmentation channels are shown in figures 4–10, which display the involved chemical structures and relative energies of transition states, intermediates and some products in the dissociation processes of MMA cation.

3.3.1. Channel 1 $C_5H_7O_2^+ + H$. In the dissociative photoionization of MMA, it can be ascertained that the fragment $C_5H_7O_2^+$ can only be produced by H elimination from the parent ion $C_5H_8O_2^+$. Since there are three types of nonequivalent H atoms located on atom C1, C3 and C7 of $C_5H_8O_2^+$, direct H abstraction from those carbon atoms is firstly taken into consideration and product ions P1a, P1b and

Table 1. Experimental, theoretical and literature values of the ionization energy (IE), appearance energy (AE) dissociation energy (Ed) and possible dissociation channels.

m/z	Ions	IE or AE (Exp.) (eV)	IE or AE (G3B3) (eV)	IE or AE (Reference) (eV)	Ed (G3B3) (eV)	Ed (Exp.) (eV)	Possible dissociation channels
100	$C_5H_8O_2^+$	9.76 ± 0.03	9.77	9.7[a]			
99	$C_5H_7O_2^+$	10.30 ± 0.03	10.49	10.4 ± 0.1[a]	0.72	0.54	$C_5H_7O_2^+ + H$
85	$C_4H_5O_2^+$	10.51 ± 0.03	10.49	10.3 ± 0.1[a]	0.72	0.75	$C_4H_5O_2^+ + CH_3$
82	$C_5H_6O^+$	10.66 ± 0.03	10.96	10.85 ± 0.1[a]	1.19	0.90	$C_5H_6O^+ + H_2O$
69	$C_4H_5O^+$	11.17 ± 0.03	11.03	10.75 ± 0.1[a]	1.26	1.41	$C_4H_5O^+ + CH_3O$
59	$C_2H_3O_2^+$	12.52 ± 0.03	12.54		2.77	2.76	$C_2H_3O_2^+ + C_3H_5$
56	$C_3H_4O^+$	10.51 ± 0.03	10.64	10.3 ± 0.1[a]	0.87	0.75	$C_3H_4O^+ + C_2H_4O$
55	$C_3H_3O^+$	10.74 ± 0.03	11.14	10.8 ± 0.1[a]	1.37	0.98	$C_3H_3O^+ + C_2H_5O$
55	$C_4H_7^+$	10.74 ± 0.03	11.03		1.26	0.98	$C_4H_7^+ + CHO_2$
41	$C_3H_5^+$	12.88 ± 0.03	12.72		2.95	3.12	$C_3H_5^+ + CH_3O + CO$
40	$C_3H_4^+$	12.73 ± 0.03	12.79		3.02	2.97	$C_3H_4^+ + C_2H_4O_2$
			12.11		2.34	2.97	$C_3H_4^+ + C_2H_2O + H_2O$
15	CH_3^+	12.82 ± 0.03	12.73		2.96	3.06	$CH_3^+ + C_4H_5O_2$

[a] [14].

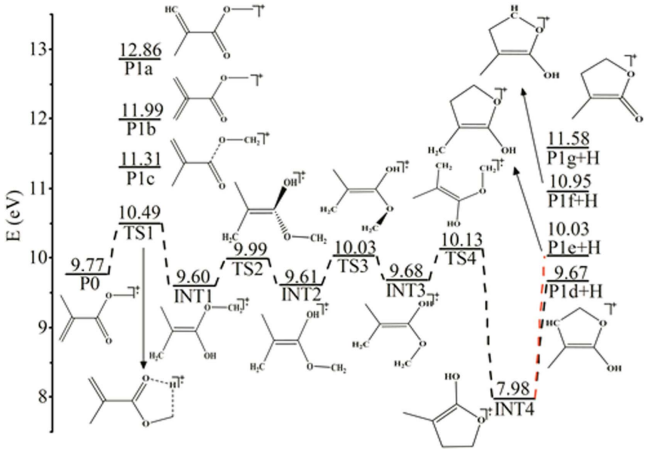

Figure 4. The dissociation pathways of the $C_5H_8O_2^+$ (P0) to produce $C_5H_7O_2^+$ (P1).

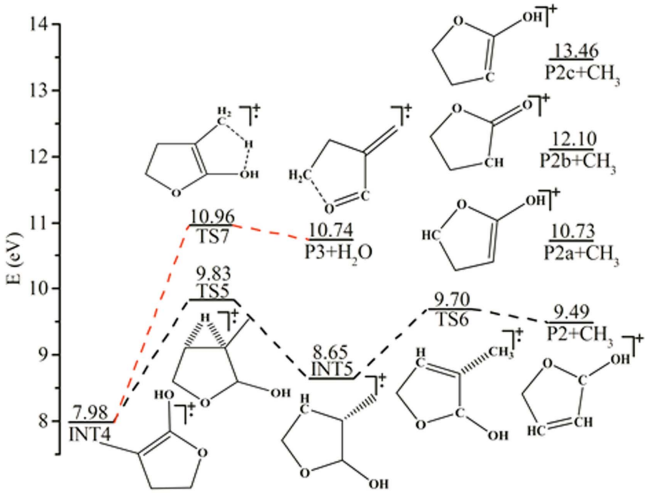

Figure 5. The dissociation pathways of the $C_5H_8O_2^+$ (P0) to produce $C_4H_5O_2^+$ (P2) and $C_5H_6O^+$ (P3).

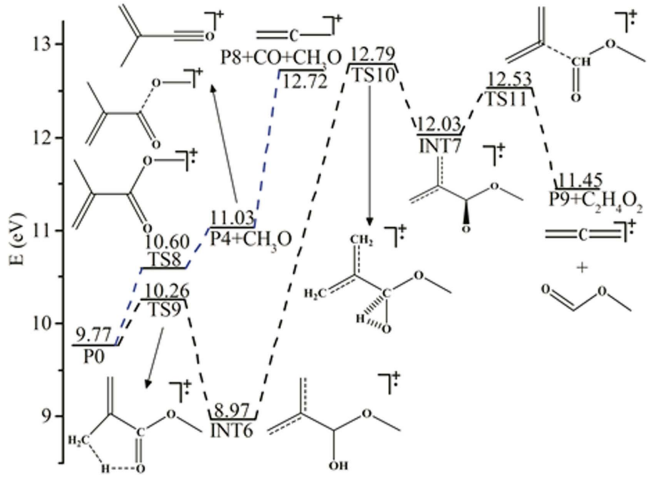

Figure 6. The dissociation pathways of the $C_5H_8O_2^+$ (P0) to produce $C_4H_5O^+$ (P4), $C_3H_5^+$ (P8) and $C_3H_4^+$ (P9).

P1c can be generated respectively. However, theoretical AEs of these three possible fragment ion isomers are 12.86, 11.99 and 11.31 eV, respectively, which are much higher than the experimental AE of $C_5H_7O_2^+$ (10.30 ± 0.03 eV). Thus, H elimination from $C_5H_8O_2^+$ is not a simple one-step bond cleavage process. Our calculations suggest a slightly more complicated mechanism, which is summarized by the energy profile shown in figure 4.

From $C_5H_8O_2^+$, firstly, one H atom from C7 can migrate to O5 via transition state TS1 with an energy barrier of 0.72 eV, forming a relatively stable intermediate INT1 which is 0.17 eV lower in energy than the molecular ion. Then, positional interchange of the OH group and the CH_2O group occurs by rotation about the C2–C4 bond, giving rise to INT2 via transition state TS2. Afterward, rotation around the C4–C6 bond transforms INT2 into intermediate INT3 wherein the two methylene groups are favorably oriented for ring closure. Subsequently, two carbon atoms C1 and C7 in INT3 come close to each other and ultimately link together to form a C–C

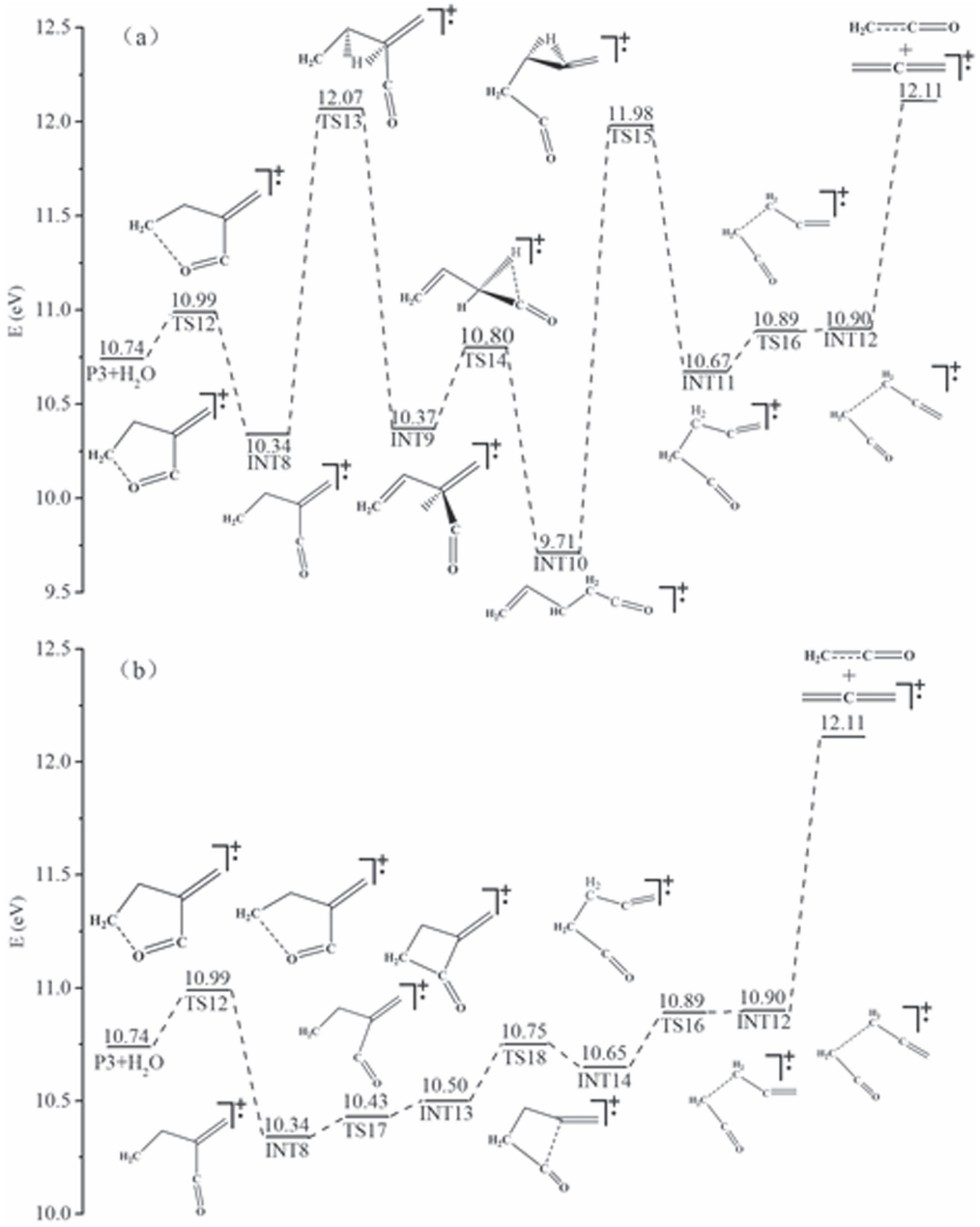

Figure 7. The dissociation pathways of $C_5H_6O^+$ (P3) to produce $C_3H_4^+$ (P9). The energies represent the sum of the energies of cation and neutral product H_2O.

single bond, leading to the formation of a more stable five-membered ring intermediate INT4. There are four types of hydrogen of widely different chemical characteristics in INT4, which may possibly be eliminated in the photodissociation process. However, the AE of $C_5H_7O_2^+$ produced by H elimination from C7 and O5 (P1f and P1g) are calculated to be 10.95 and 11.58 eV, respectively, clearly too high to be considered here. Whereas elimination of the hydrogen atom belonging to C1 and C3 gives $C_5H_7O_2^+$ (P1d and P1e) with relative energy of 9.67 and 10.03 eV, respectively, both of which are lower in energy than TS1, the highest energy step along the entire pathway, whose relative energy is close to the experimental AE value for fragment ion at $m/z = 99$. Thus, it can be confirmed that both P1d and P1e are energetically possible products. The cleavage of C–H bond in INT4 is regarded to be barrierless, no distinct transition state exists on the potential energy surface.

3.3.2. Channel 2 $C_4H_5O_2^+ + CH_3$. For the formation of $C_4H_5O_2^+$, obviously there are two nonequivalent methyl groups in the parent ion and direct elimination one of the two methyl groups are firstly considered, similarly to the case of H elimination in channel 1. The theoretical AEs of products generated by C3 methyl elimination and C7 methyl elimination are calculated to be 12.54 and 14.26 eV respectively, which are both much higher compared with the experimental value 10.51 ± 0.03 eV. It is thus clear that direct elimination of methyl group to produce $C_4H_5O_2^+$ could

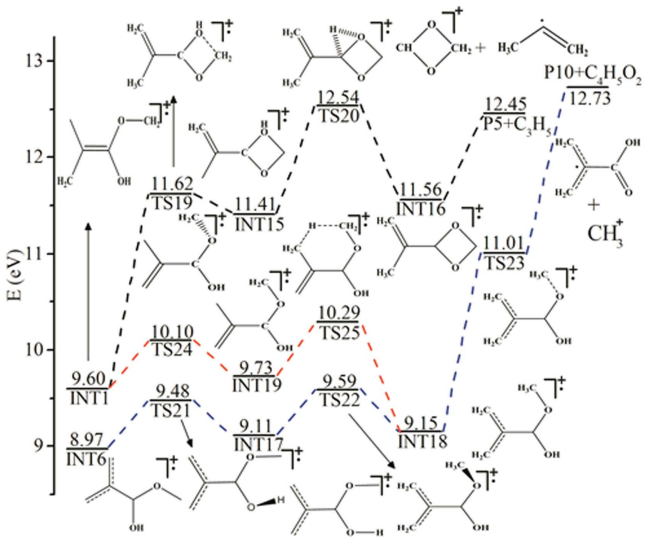

Figure 8. The dissociation pathways of the $C_5H_8O_2^+$ (P0) to produce $C_2H_3O_2^+$ (P5) and CH_3^+ (P10).

be excluded here. We then proposed an energetically feasible pathway involving hydrogen migrations and ring-formation, which is shown in detail in figure 5. Starting from the five-membered ring intermediate INT4 formed as described in channel 1, one hydrogen atom of C1 is transferred to C2 via transition state TS5, leading to the formation of intermediate INT5. Subsequently, the loss of C2 methyl occurs via transition state TS6 to generate P2 through bond cleavage of C2–C3, which is elongated to 2.331 Å in TS6 from 1.556 Å in INT5. According to theoretical calculations, TS1 is the highest energy step along the entire pathway, which is the same situation as in channel 1, and the corresponding dissociation energy is 0.72 eV, showing good agreement with the experimental Ed value 0.75 eV. It should be mentioned that the possibility of producing $C_4H_5O_2^+$ (P2c) through direct cleavage of the methyl group in INT4 can be ruled out in this study because it requires activation energy of at least 13.46 eV according to G3B3 computations. In addition, the other two $C_4H_5O_2^+$ isomers, P2a and P2b, which are produced involving migration of the hydrogen atoms of C7 and O5, could also be safely ignored as they need energy of at least 10.70 and 12.10 eV, respectively.

3.3.3. Channel 3 $C_5H_6O^+ + H_2O$. On the basis of the computational results, we suggest that the fragment at $m/z = 82$ may have the chemical formula of $C_5H_6O^+$ and is produced with the release of H_2O from the molecular ion. From INT4, which is formed via a series of arrangement steps as shown in figure 5, one hydrogen atom of the methyl group can migrate to the hydroxyl group, passing through transition state TS7 with an energy barrier of 2.98 eV. Comparisons of IRC computations and independent optimizations of TS7 show that there is no further intermediate or transition state prior to the cleavage of the C4–O5 bond, indicating that hydrogen migration and cleavage of C–O bond occurs simultaneously for INT4 at the G3B3 theoretical level, which is consistent with computations of similar systems [23]. Regarding the energy of TS7 as the theoretical AE, which is predicted to be 10.96 eV, it is in rough agreement with our experimental value of 10.66 ± 0.03 as well as the literature value of 10.85 ± 0.1 eV.

3.3.4. Channel 4 $C_4H_5O^+ + CH_3O$ ($C_3H_5^+ + CH_3O + CO$). Considering the fact that the ester functional group (–COO–) is derived from carboxyl group (–COOH) and hydroxyl group (–OH) by dehydration-condensation reaction and direct bond cleavage of the ester functional group of ethyl acrylate has been reported [23], it is thus reasonable to infer in the first place, that fragment ion $C_4H_5O^+$ may be produced by bond scission of C4–O6 of the parent ion. Theoretical AE for the product ion P4 is predicted to be 11.03 eV, in excellent accord with our experimental value of 11.17 ± 0.03 eV, thus confirming the above inference. Detailed formation pathway of P4 with potential energy surface is depicted in figure 6. From parent ion $C_5H_8O_2^+$, P4 can be formed via transition state TS8 with an energy barrier of 0.83 eV. Along the pathway, the C4–O6 bond length is stretched, resulting in the loss of CH_3O radical. IRC computations show that there is no further minimum prior to the cleavage of the C4–O6 bond at the G3B3 level. It should be mentioned here that formation of $C_4H_5O^+$ along with methanal from dissociation of fragment $C_5H_7O_2^+$ has also been taken into consideration. Considering the geometry of $C_5H_7O_2^+$, $C_4H_5O^+$ ion may have the structural formula CH_3CCH_2CO (P4), CH_2CCH_2COH or $CH_2CHCHCOH$; the corresponding AEs are calculated to be at least 22.76, 24.50 and 24.84 eV, respectively. Thus, the dissociation channel $C_5H_7O_2^+ \rightarrow C_4H_5O^+ + CH_2O$ is not energetically favorable and should not occur in our experiments.

The fragment ion $C_3H_5^+$, whose structure and stability has been theoretically investigated previously [24], is tentatively assigned to 2-propenyl cation in this study. For the formation pathway of $C_3H_5^+$, we first consider the possibility of producing $C_3H_5^+$ by direct breakage of the C2–C4 bond. According to G3B3 calculations, AE for $C_3H_5^+$ produced through this way is predicted to be 12.05 eV, which is 0.83 eV lower than the experimental AE. Thus, formation of $C_3H_5^+$ should proceed through more complicated channels. Then, two sequential fragmentation reactions, $C_5H_8O_2^+ \rightarrow C_5H_7O_2^+ \rightarrow C_3H_5^+$ and $C_5H_8O_2^+ \rightarrow C_4H_5O_2^+ \rightarrow C_3H_5^+$, have been considered. The first reaction, producing $C_3H_5^+$ along with neutral product glyoxal ($C_2H_2O_2$), can be discarded since the minimum required energy is 13.69 eV. The latter reaction, generating $C_3H_5^+$ with the release of CO_2, is calculated to occur at least at 11.30 eV, which is 1.58 eV lower than our experimental AE for $C_3H_5^+$. Theoretically, this energy difference may be due to the need to overcome a high-energy transition state involved in the reaction pathway. However, despite many efforts, no energetically permitted pathway can be found, implying that this fragmentation reaction is unlikely to occur during the photoionization process. Finally, $C_3H_5^+$ is proposed to be formed from further dissociation of P4, accompanied by loss of CO. We have scanned the C2–C4

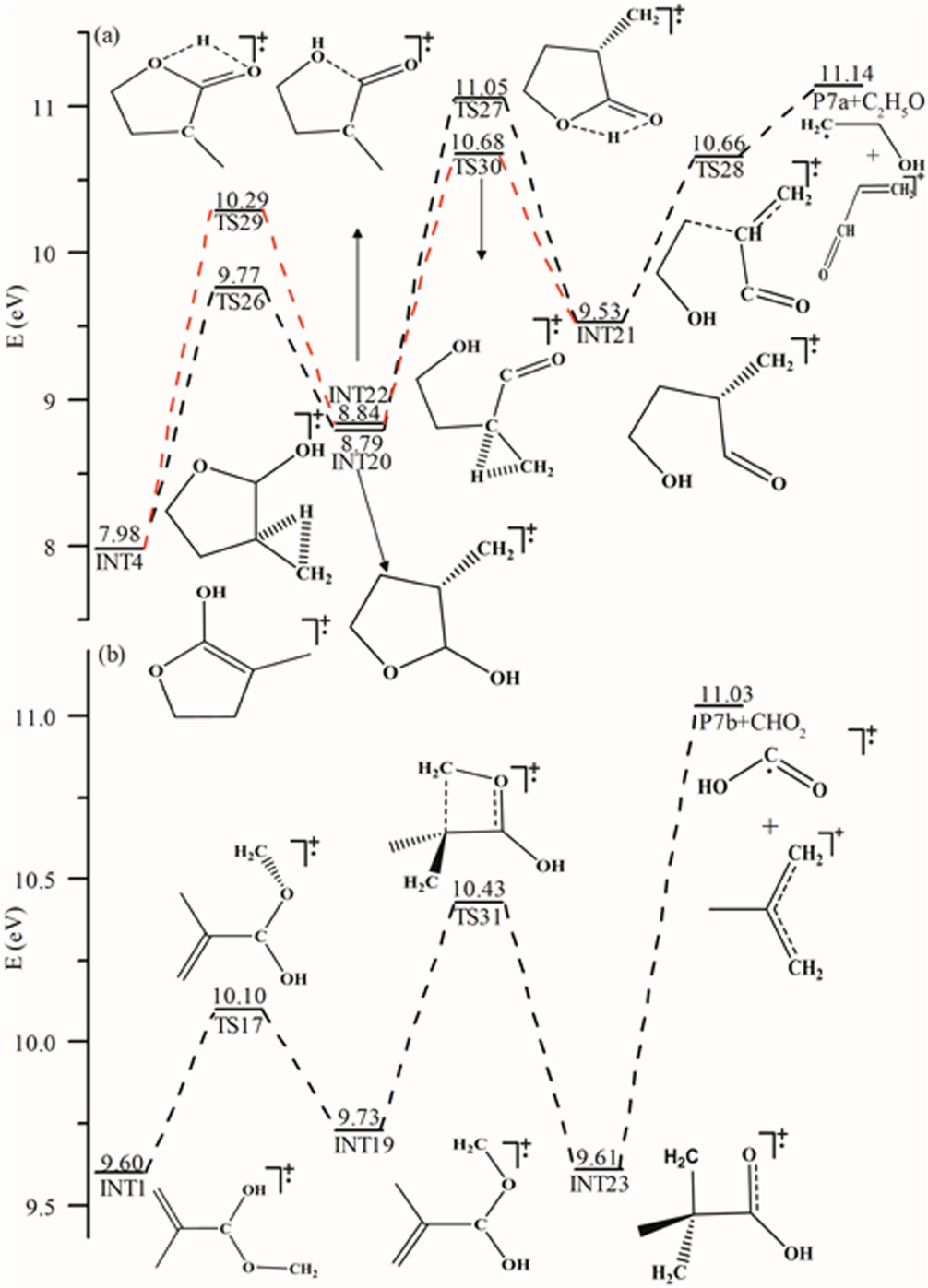

Figure 9. The dissociation pathways of the $C_5H_8O_2^+$ (P0) to produce $C_3H_3O^+$ (P7a) and $C_4H_7^+$ (P7b).

bond length from 1.5 to 3.1 Å and found no possible transition state, indicating that elimination of CO from P4 is a simple bond cleavage process. It is noteworthy that fragment ions P4 and P8 correspond to peaks of the highest intensity both in the 14 eV PIMS and in the 70 eV EIMS [20], implying that cleavage of the C–O bond plays an important role in the fragmentation of MMA.

3.3.5. Channel 5 $C_3H_4^+ + C_2H_4O_2$. The peak at $m/z = 40$ corresponds to $C_3H_4^+$, which is tentatively assigned to the allene radical cation on the basis of computational results. As shown in figure 6, for the formation pathway of allene radical cation from the molecular ion, one H atom of C3 can firstly migrate to O5 via transition state TS9, leading to the formation of intermediate INT6. Due to the delocalization of the unpaired electron along the C=C double bond, INT6 is found to be more stable than the molecular ion by 0.80 eV. Subsequently, the hydrogen atom at O5 atom of INT6 is transferred to the C4 atom to produce intermediate INT7. Because of the lack of charge delocalization along the O=C–O bond, INT7 is found to be 12.03 eV high in energy and the transformation process involves a high-energy barrier of

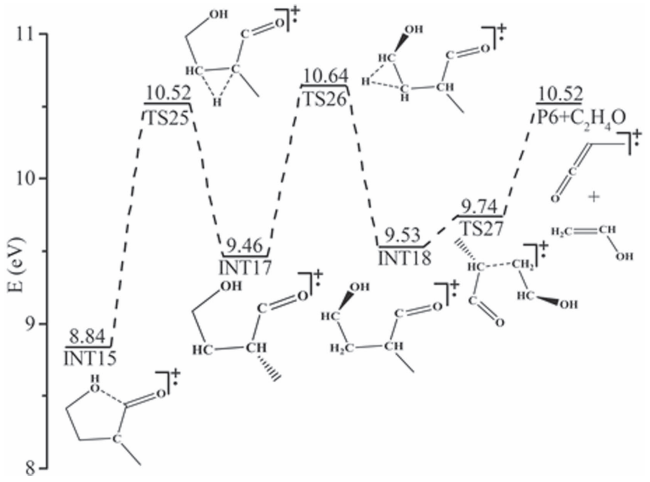

Figure 10. The dissociation pathways of the $C_5H_8O_2^+$ (P0) to produce and $C_3H_4O^+$ (P6).

3.82 eV. Finally, direct bond cleavage of C2–C4 in INT7 via transition state TS11 gives allene cation as final product, accompanied by the release of methyl formate. Regarding the energy of TS10 (12.79 eV), the highest energy step along the entire pathway, as the calculated barrier, it is in good agreement with the observed value of 12.73 ± 0.03 eV.

Besides the pathway discussed above, there are two alternative pathways that may also lead to the formation of allene radical cation. As described in figure 7(a), P3 can first ring-open to give INT8 via TS12 with an energy barrier of 0.25 eV. Afterward, INT8 undergoes a 1,2-H migration to produce INT9 which can rearrange to INT10 via a carbonyl group migration. INT10 then isomerizes to INT11 via a 1,2-H shift, passing through TS15 whose relative energy is 11.98 eV. Finally, INT11 has its CH_2–CH_2 bond cleaved through TS16 to yield INT12, which dissociates to produce allene radical cation and ethenone. As shown in figure 7(b), in addition to undergoing hydrogen migration, INT8 can cyclize to form four-membered ring intermediate INT12, which can isomerize to INT12 through a ring-opening step followed by a CH_2–CH_2 bond cleavage process. It can be seen that these two pathways have the same theoretical AE (12.11 eV). Since the calculated AE for the channel $C_5H_8O_2^+ \rightarrow C_3H_4^+ + C_2H_4O_2$ is more close to the experimental value, we think that formation of allene radical cation from the molecular ion is more reasonable.

3.3.6. Channel 6 $C_2H_3O_2^+ + C_3H_5$. At first glance, one might think that $C_2H_3O_2^+$ can be readily produced from a simple C2–C4 bond rupture of the parent ion, accompanied by the release of the C_3H_5 radical. However, the resulting structure of ionic fragment could not be located at the G3B3 level, indicating that formation of $C_2H_3O_2^+$ from MMA should proceed through a more complicated mechanism. Superficially, $C_2H_3O_2^+$ may also be produced by dissociation reactions $C_5H_7O_2^+ \rightarrow C_2H_3O_2^+ + C_3H_4$ and $C_4H_5O_2^+ \rightarrow C_2H_3O_2^+ + C_2H_2$. For the first reaction, neutral product C_3H_4 may be propyne (CH_3CCH) or allene (CH_2CCH_2); the AEs of $C_2H_3O_2^+$ produced are calculated to be 13.96 and 14.01 eV, respectively. The latter reaction is also not favored in terms of energy, as it requires energy of 13.76 eV or higher. Therefore, formation of $C_2H_3O_2^+$ from dissociation of fragment ions $C_5H_7O_2^+$ and $C_4H_5O_2^+$ can be excluded. According to our theoretical calculations, an energetically feasible pathway is then proposed which is displayed in detail in figure 8. First, parent ion undergoes a 1,4-hydrogen shift to yield the intermediate INT1 overcoming a barrier of 0.72 eV as shown in channel 1. Then, a four-membered ring intermediate INT15 is produced via transition state TS19, wherein the distance between C7 and O5 is shortened. Subsequently, an intramolecular 1,2-hydrogen transfer process occurs from O5 to C4 to transform INT15 into INT16 via transition state TS20. The final product P5 is yielded by breaking the C2–C4 bond in INT16, accompanied with the loss of C_3H_5 radical.

3.3.7. Channel 7 $CH_3^+ + C_4H_5O_2$. At first sight, the methyl cation corresponding to the peak at $m/z = 15$ can be readily produced from a simple cleavage of C3 or C7 in the molecular ion. However, G3B3 theoretical calculations show that CH_3^+ yielded through this way would have the appearance energy of 14.30 and 13.67 eV, respectively, which are too high as compared with the experimental AE value of 12.82 ± 0.03 eV, indicating the formation of methyl radical from MMA should involve a series of isomerization steps. Intuitively, one may think CH_3^+ could be generated from $C_5H_7O_2^+$ with the release of $C_4H_4O_2$. However, this channel can be discarded because its reaction barrier (at least 14.36 eV) is too high with respect to the experimental value. Similarly, the dissociation channel $C_4H_5O_2^+ \rightarrow CH_3^+ + C_3H_2O_2$ to produce CH_3^+ and propionic acid (CHCCOOH) can also be ignored due to its high threshold (greater than or equal to 14.97 eV). Another possible channel is $C_2H_3O_2^+ \rightarrow CH_3^+ + CO_2$, which is computed to occur at least at 13.23 eV. However, considering the geometry of $C_2H_3O_2^+$, G3B3 calculations revealed that dissociation of would produce HCO cation plus methanal (HCOH) or CH_2OH cation plus CO, rather than CH_3^+ and CO_2. Thus, this channel is not likely to take place in the photodissociation experiment.

The results of our computations suggest a plausible formation pathway which is depicted in figure 8. Starting from INT6, rotation around the C4–O5 bond via transition state TS21 can generate INT17, an intermediate which is slightly less stable than INT6 because of the steric hindrance between the methyl group and the hydroxyl group. Afterward, rotation about the C4–O6 bond transforms INT17 into intermediate INT18. Herein, an alternative formation route for INT18 is found, that is, rotation about the C4–O6 bond in INT1 followed by a 1,5-hydrogen migration step between the C3 atom and the C7 atom, via INT19 as the intermediate. The transition states involved, TS24 and TS25, possess a relative energy of 10.10 and 10.29 eV, respectively. Finally, INT18 dissociates to produce methyl cation through bond fission of C7–O6, passing through transition state TS23 with an energy barrier of 1.86 eV.

3.3.8. Channel 8 $C_3H_3O^+ + C_2H_5O$ and $C_4H_7^+ + CHO_2$. There are two possible candidate structures, $C_3H_3O^+$ and $C_4H_7^+$ (labeled as P7a and P7b), that can be assigned to the peak at $m/z = 55$ according to *ab initio* calculations at G3B3 level. Detailed formation pathways with potential energy diagram are depicted in figure 9.

In the case of $C_3H_3O^+$, starting from the molecular ion, a 1,4-H migration followed by a ring closure leads to the formation of INT4 which has been shown in figure 3. For the sake of brevity, these steps are not displayed in figure 9(a), where only the remaining part of the pathway proceeding from INT4 is depicted. The first step is a 1,2-H migration from the CH_3 group to the neighboring hydrogen-less carbon, leading to less stable intermediate INT20 via a barrier of 1.79 eV. INT20 can subsequently experience another hydrogen shift from O5 to O6 coupled with a bond fission of C4–O6, giving a ring-opening intermediate INT21. Such a process involves a high-energy barrier of 2.26 eV. Alternatively, from INT4, INT21 can be produced through hydrogen migration from O5 to O6 accompanied with C4–C6 bond cleavage, followed by another hydrogen shift from C3 to C2 of INT22, which is the intermediate involved in the process. The corresponding transition states, TS29 and TS30, are computed to be 0.76 and 0.37 eV lower in energy than TS27, indicating that INT21 formation in this pathway is energetically more favorable than the former INT4 → TS26 → INT20 → TS27 → INT21 route. Subsequently, INT21 proceeds to produce $C_3H_3O^+$ and C_2H_5O by overcoming a barrier of 1.13 eV via transition state TS28.

As shown in figure 9(b), for the formation of $C_4H_7^+$, firstly, rotation around the O6–C7 bond can transform INT1 into isomer INT19, with the latter less stable than the former by 0.13 eV due to the steric hindrance posed by the CH_3 group. Notably, the greatest change in geometry is observed in the dihedral angle of C2–C4–O6–C7 (see Supporting Information, figures S2 and S3), which varies from −170.96° (INT1) to 18.69° (INT19) as compared to −97.30° in the corresponding transition state, TS24, which possesses a relative energy of 10.10 eV. Secondly, INT19 can proceed to undergo a 1,3-methylene transfer to yield a more stable intermediate, INT23, passing through transition state TS31 with an energy barrier of 0.70 eV. Lastly, with the release of COOH radical through cleavage of the C2–C4 bond in INT23, the final product of 2-methylallyl cation is yielded, which has been proven to be a stable isomer of $C_4H_7^+$ [25]. The overall barrier for this formation pathway is calculated to be 11.03 eV, showing reasonable agreement with our experimental result.

It should be mentioned here that we also performed theoretical calculations for formation of $C_3H_4O^+$ from dissociation of fragment ions $C_5H_7O_2^+$ and $C_4H_5O_2^+$. For reaction $C_5H_7O_2^+ \rightarrow C_3H_3O^+ + C_2H_4O$, neutral product C_2H_4O may be acetaldehyde (CH_3COH), ethylene oxide (CH_2OCH_2), or ethanol (CH_2CHOH). The reaction barrier for these three reaction pathways are computed to be at least 11.90, 13.10, and 12.34 eV, which are much higher than the experimental AE of 10.74 eV for $C_3H_3O^+$. Dissociation of $C_4H_5O_2^+$ to $C_3H_3O^+$ with the release of methanal is also a high-energy process; the reaction barrier is calculated to be at least 22.58 eV. Thus, we can rule out formation pathways of $C_3H_4O^+$ from dissociation of fragment ions in our study. In the case of $C_4H_7^+$, dissociation reaction $C_5H_7O_2^+ \rightarrow C_4H_7^+ + CO_2$ has been investigated. In view of the geometry of P1d and P1e, $C_4H_7^+$ produced should be $CH_3CCH_3CH_3$ (P7b) and $CH_3CHCHCH_2$, respectively; the corresponding AE are calculated to be at least 10.91 and 10.49 eV, which is close to the experimental value of 10.74 eV. However, no energetically favorable formation pathway of $C_4H_7^+$ from this reaction could be located at the G3B3 level.

3.3.9. Channel 9 $C_3H_4O^+ + C_2H_4O$. The species at m/z 56 is assigned to $C_3H_4O^+$, theoretical calculations suggest that this ion corresponds to methylketene radical cation, the probable dissociation pathway being: $C_5H_8O_2 + h\nu \rightarrow C_3H_4O^+ + C_2H_4O$. This pathway is actually branched from channel 8 and the corresponding energy profile is displayed in figure 10. Besides isomerization to produce intermediate INT21 through hydrogen shift as described in figure 9(a), INT22 can also be transformed into intermediate INT24 through transition state TS32 via a 1,2-hydrogen migration between C1 and C2 atoms. Once INT24 is formed, it can proceed to undergo another 1,2-hydrogen shift via transition state TS33. The product ion, INT25, possessing a relative energy of 9.53 eV, has comparable stability with INT24. The generated C1–C2 bond is elongated to 2.187 Å in TS34 from 1.59 Å in INT25. Finally, methylketene radical cation is yielded with concomitant elimination of ethanol through breakage of the C1–C2 bond, and no stable ion-neutral complex is found at the G3B3 level.

4. Conclusions

VUV photon-induced ionization and fragmentation of MMA have been investigated by the combined techniques of molecular beam, SR and TOF mass spectrometry. IE of MMA and AEs of main fragment ions $C_5H_7O_2^+$, $C_5H_6O^+$, $C_4H_5O_2^+$, $C_4H_5O^+$, $C_3H_4O^+$, $C_3H_3O^+$ ($C_4H_7^+$), $C_3H_5^+$, $C_3H_4^+$, $C_2H_3O_2^+$, and CH_3^+ are obtained by measuring the PIE spectrum. With the aid of G3B3 theoretical calculation, dissociative photoionization channels $C_5H_7O_2^+ + H$, $C_5H_6O^+ + H_2O$, $C_4H_5O_2^+ + CH_3$, $C_4H_5O^+ + CH_3O$ ($C_3H_5^+ + CH_3O + CO$), $C_2H_3O_2^+ + C_3H_5$, $C_3H_4O^+ + C_2H_4O$, $C_3H_3O^+ + C_2H_5O$ ($C_4H_7^+ + CHO_2$), $C_3H_4^+ + C_2H_4O_2$, $C_3H_4^+ + C_2H_2O + H_2O$ and $CH_3^+ + C_4H_5O_2$ are proposed and discussed in detail. Hydrogen shift and ring closing/opening processes dominate most of the fragmentation pathways of the MMA cation. This work will be helpful to better understand the fragmentation pathways of MMA and similar α,β-unsaturated esters.

Acknowledgments

This work has been supported by the grants from the National Nature Science Foundation of China (U1232209, U1232130, 41275127, and 11575178). The authors are grateful to the Supercomputing Center of University of Science and Technology of China for generous allocation of computing resources.

ORCID iDs

Jun Chen https://orcid.org/0000-0002-4832-0375

References

[1] Brune D and Beltesbrekke H 1981 Levels of methylmethacrylate, formaldehyde, and asbestos in dental workroom air *Scand. J. Dent. Res.* **89** 113–6

[2] Nagai K 2001 New developments in the production of methyl methacrylate *Appl. Catal. A: Gen.* **221** 367–77

[3] Hirata T, Kashiwagi T and Brown J E 1985 Thermal and oxidative-degradation of poly(methyl methacrylate)—weight-loss *Macromolecules* **18** 1410–8

[4] Zeng W R, Li S F and Chow W K 2002 Review on chemical reactions of burning Poly(methyl methacrylate) PMMA *J. Fire Sci.* **20** 401–33

[5] Lin Z K, Wang T F, Han D L, Han X, Li S F, Li Y Y and Tian Z Y 2009 Study of combustion intermediates in fuel-rich methyl methacrylate flame with tunable synchrotron vacuum ultraviolet photoionization mass spectrometry *Rapid Commun. Mass Spectrom.* **23** 85–92

[6] Canosa-Mas C E, Carr S, King M D, Shallcross D E, Thompson K C and Wayne R P 1999 A kinetic study of the reactions of NO_3 with methyl vinyl ketone, methacrolein, acrolein, methyl acrylate and methyl methacrylate *Phys. Chem. Chem. Phys.* **1** 4195–202

[7] Grosjean D, Grosjean E and Williams E L 1993 Rate constants for the gas-phase reactions of ozone with unsaturated alcohols, esters, and carbonyls *Int. J. Chem. Kinet.* **25** 783–94

[8] Wang K, Ge M F and Wang W G 2010 Kinetics of the gas-phase reactions of NO_3 radicals with ethyl acrylate, n-butyl acrylate, methyl methacrylate and ethyl methacrylate *Atmos. Environ.* **44** 1847–50

[9] Blanco M B, Bejan I, Barnes I, Wiesen P and Teruel M A 2014 Products and mechanism of the reactions of OH radicals and Cl atoms with methyl methacrylate (CH_2=C(CH_3)C(O)OCH_3) in the presence of NO_x *Environ. Sci. Technol.* **48** 1692–9

[10] Blanco M B, Bejan I, Barnes I, Wiesen P and Teruel M A 2009 Temperature-dependent rate coefficients for the reactions of Cl atoms with methyl methacrylate, methyl acrylate and butyl methacrylate at atmospheric pressure *Atmos. Environ.* **43** 5996–6002

[11] Gibilisco R G, Uranga J G, Santiago A N and Teruel M A 2015 Atmospheric degradation of CH_2=C(CH_3)C(O)OCH_3 initiated by OH radicals: mechanistic study and quantification of $CH_3C(O)C(O)OCH_3$ in NO_x free air *J. Phys. Chem.* A **119** 8775–83

[12] Sustmann R and Trill H 1972 Photoelektronenspektroskopische bestimmung von substituenten-effekten II. α,β-ungesättigte carbonester *Tetrahedron Lett.* **13** 4271–4

[13] Van Dam H and Oskam A 1978 He(I) and He(Ii) photoelectron-spectra of some substituted ethylenes *J. Electron. Spectrosc.* **13** 273–90

[14] Wang J, Yang B, Cool T A and Hansen N 2010 Absolute cross-sections for dissociative photoionization of some small esters *Int. J. Mass. Spectrom.* **292** 14–22

[15] Wang S S, Kong R H, Shan X B, Zhang Y W, Sheng L S, Wang Z Y, Hao L Q and Zhou S K 2006 Performance of the atomic and molecular physics beamline at the National Synchrotron Radiation Laboratory *J. Synchrotron Radiat.* **13** 415–20

[16] Fang W Z, Gong L, Zhang Q, Shan X B, Liu F Y, Wang Z Y and Sheng L S 2011 Dissociative photoionization of 1,3-butadiene: experimental and theoretical insights *J. Chem. Phys.* **134** 174306

[17] Chen J, Cao M Q, Wei B, Ding M M, Shan X B, Liu F Y and Sheng L S 2016 Vacuum ultraviolet photoionization mass spectrometric study of cyclohexene *J. Mass Spectrom.* **51** 169–81

[18] Frisch M J *et al* 2009 Gaussian 09 Revision A.02, Gaussian, Inc., Wallingford, CT, USA

[19] Baboul A G, Curtiss L A, Redfern P C and Raghavachari K 1999 Gaussian-3 theory using density functional geometries and zero-point energies *J. Chem. Phys.* **110** 7650–7

[20] Lias S G, Levin R D and Kafafi S A 2016 *Ion Energetics Data in NIST Chemistry WebBook, NIST Standard Reference Database Number 69* ed P J Linstrom and W G Mallard (Gaithersburg, MD 20899: National Institute of Standards and Technology) http://webbook.nist.gov

[21] Chiang S Y, Bahou M, Sankaran K, Lee Y P, Lu H F and Su M D 2003 Dissociative photoionization of CH_2Cl_2 and enthalpy of formation of $CHCl^+$: experiments and calculations *J. Chem. Phys.* **118** 62–9

[22] Wilson K R, Belau L, Nicolas C, Jimenez-Cruz M, Leone S R and Ahmed M 2006 Direct determination of the ionization energy of histidine with VUV synchrotron radiation *Int. J. Mass Spectrom.* **249** 155–61

[23] Song Y L, Chen J, Ding M M, Wei B, Cao M Q, Shan X B, Zhao Y J, Huang C Q, Sheng L S and Liu F Y 2015 Dissociative photoionization of ethyl acrylate: theoretical and experimental insights *J. Mol. Struct.* **1094** 83–90

[24] Bowen R D, Williams D H, Schwarz H and Wesdemiotis C 1979 Energy barriers for isomerization of gaseous $C_3H_5^+$ ions *J. Am. Chem. Soc.* **101** 4681–3

[25] Koch W, Liu B and Defrees D J 1988 The $C_4H_7^+$ cation—a theoretical investigation *J. Am. Chem. Soc.* **110** 7325–8